Mon. Not. R. Astron. Soc. **000**, 000–000 (0000) Printed January 31, 2017 (MN LATEX style file v2.2)

Radio spectral index from NVSS and TGSS

Prabhakar Tiwari[1] ⋆
[1] *Department of Physics, Technion - Israel Institute of Technology, Haifa 32000, Israel*

January 31, 2017

arXiv:1609.01308v2 [astro-ph.GA] 27 Jan 2017

ABSTRACT

We extract the radio spectral index, α, from 541,195 common sources observed in the 150 MHz TIFR GMRT Sky Survey (TGSS) and the 1.4 GHz NRAO VLA Sky Survey (NVSS). This large common source catalog covers about 80% of the sky. The flux limits in these surveys are such as the observed galaxies are presumably hosts of active galactic nuclei (AGNs). We confirm the steepening of α with increasing flux density for this large sample and provide a parametric fit between α and flux density. Next, we divide the data into a low flux (LF) and a high flux (HF) sample of roughly equal number of galaxies. The LF sample contains all galaxies below 100 mJy TGSS and 20 mJy NVSS flux density and the HF sample is all galaxies above 100 mJy TGSS and 20 mJy NVSS. We observe an increase in α with source size (TGSS measured), saturating for large sizes to 0.89 ± 0.01 and 0.76 ± 0.00 for the LF and HF sources, respectively. For the most compact sources in the LF sample $\alpha < 0.4$, indicating a significant contribution from thermal emission. We discuss the observed results and possible physical mechanisms to explain observed α dependence with source size for LF and HF samples.

Key words: galaxies: high-redshift, galaxies: active galactic nuclei

1 INTRODUCTION

The radio emission from a distant galaxy consists of thermal and synchrotron contributions. The thermal emission is bremsstrahlung radiation from HII regions while the non-thermal synchrotron emission is generated by supernova remnants (SNRs), diffuse cosmic ray electrons (CREs) spread over the disk and halo (Biermann 1976; Condon 1992), relativistic plasma in jets and jet fed lobes(De Young 1976; Blandford & Königl 1979). The bright radio galaxies, relevant to flux limits in this work, are hosts of AGNs and their radio emission is predominantly synchrotron radiation from jets of relativistic plasma and jet fed lobes. These emission components are characterized by different spectral indices and, therefore, the total spectral index depends on their relative contributions. The thermal emission is almost flat ($\propto \nu^{-\alpha}$) with spectral index $\alpha_{_{\rm th}} \approx 0.1$(Condon 1992), whereas, the radio jets exhibit a spectral index $\alpha_{_{\rm jet}} = 0.5-0.9$ (Bridle & Perley 1984) and the radio emission from lobes can be flat to very steep depending on energy injection and losses (Kellermann 1966).

We compile a unique source catalog from TIFR GMRT Sky Survey (TGSS)(Intema et al. 2016) and NRAO VLA Sky Survey (NVSS)(Condon et al. 1998), and use it to explore radio spectral index size and flux dependence. We identify a total of 541,195 sources which are common to both TGSS and NVSS. The large sample allows us to extract spectral index in differential source size bins and we obtain statistically significant dependence of spectral index on flux density and size. Assuming that the NVSS source population peaks between redshift $z \approx 0.5-1$ (Wilman et al. 2008; Nusser & Tiwari 2015; Tiwari & Nusser 2016), all results in this work statistically represents the radio source population at redshift $z \approx 0.8$.

The outline of the paper is as following. We discuss the NVSS and TGSS data and describe the cross matching procedure in Section 2. In Section 3 we discuss the basic mechanisms of radio emission and their spectral index. We describe the observed spectral index in Section 4. In Section 5 we give all our results. We conclude with discussion in Section 6.

2 DATA

2.1 TGSS

The TGSS catalog is based on the Giant Metrewave Radio Telescope (GMRT), performing all-sky radio continuum survey at 150 MHz (Swarup 1991). The catalog is surveyed between 2010 and 2012 and has been published recently by Intema et al. (2016). The catalog covers 90% of the full sky at 150 MHz with median RMS brightness fluctuations 3.5 mJy/beam at resolution 25″x 25″north of 19°

⋆ ptiwari@physics.technion.ac.il

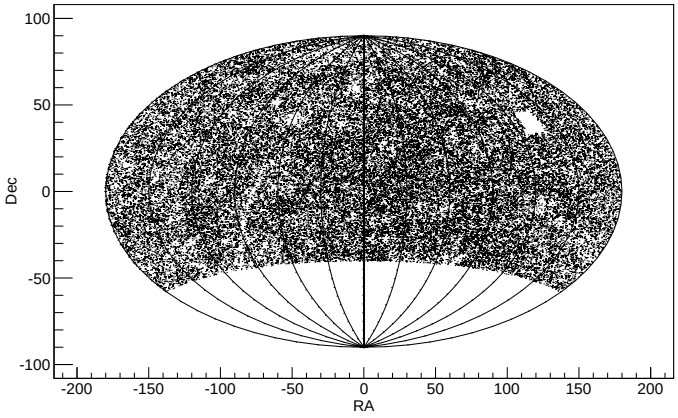

Figure 1. The spatial distribution of NVSS-TGSS common sources. Only 10% randomly selected sources are plotted.

DEC and 25″x 25″/cos(DEC-19°) south of 19°. The catalog contains a total 623,604 sources (489,570 sources above flux 50 mJy) observed at 6σ peak-to-noise threshold. The accuracy of the source centroid position is better than 2″(RMS) (Intema et al. 2016).

2.2 NVSS

The NVSS catalog contains ∼1.7 million sources at 1.4GHz with fluxes $S_{1.4\rm GHz} > 2.5$ mJy (Condon et al. 1998). This flux limit roughly corresponds the TGSS fluxes (at 150 MHz). The full width at half maximum angular resolution is 45″and nearly all observations are performed at uniform sensitivity. The catalog covers about 82% of the sky and has a 100% overlap with TGSS. The RMS uncertainty in angular position is up to 7″, substantially larger than TGSS.

2.3 TGSS-NVSS common source catalog

Given the TGSS angular position of each of the 623,604 TGSS sources, we identify NVSS sources within an angular distance less than 30″. In total we find 553,301 TGSS sources having at least one NVSS source within 30″. A few of the TGSS sources have more than one NVSS association with our search criteria of 30″, we drop these to avoid confusion and artificial scatter in the spectral index. We end up with a total 541,195 unique sources, identified in both TGSS and NVSS. The spatial distribution of these common sources is shown in Fig.1.

3 RADIO EMISSIONS IN AGNS

3.1 Thermal radio emission from H II regions

The flux density of radio thermal emission dependence on frequency is expressed as (Condon 1992),

$$S_T \propto \nu^{-0.1} \ . \tag{1}$$

At high frequencies (∼ GHz) where the electron deflection opacity is small, the ratio of the non-thermal emission approximate thermal radio emission S_T with respect to non-thermal radio emission $S_{\rm NT}$ is (Condon & Yin 1990),

$$S_{\rm NT} \sim 10 \left(\frac{\nu}{\rm GHz}\right)^{0.1-\alpha} S_T, \tag{2}$$

where $\alpha \sim 0.8$ is the approximate non-thermal spectral index. This implies that the non-thermal emission is dominant with a thermal contribution of $\lesssim 10\%$ at 1.4 GHz and $\lesssim 3\%$ at 150 MHz.

3.2 Non-thermal radio emission

3.2.1 Radio emission from Jets

Electrons in plasma of jets generated by AGNS are accelerated continuously. Their number distribution is expressed as $N(E) \propto E^{-\gamma}$, where $\gamma \approx 2$ (Blandford & Königl 1979). The radio emission from such relativistic jet is $\alpha_{\rm jet} = (\gamma - 1)/2$ i.e. for $\gamma = 2$, $\alpha_{\rm jet} = 0.5$. A realistic jet, however, emits radiation with spectral index $\alpha_{\rm jet} = 0.5 - 0.9$ (Bridle & Perley 1984).

3.2.2 Radio emission from Jet fed lobes

The radio emission from extended radio-loud galaxies is dominant by radio lobes which are fed by collimated narrow jets. The radio emission from these lobes depends on electron injection and energy losses. For a continuous supply of electrons, the number distribution obtained by considering losses to synchrotron is $N(E) \propto E^{-1-\gamma}$ (Kellermann 1966), corresponding to $\alpha = \gamma/2$. If the energy injection is intermittent, then α depends on the frequency ν and the time interval between the bursts. In this case, the radio emission can be very flat ($\alpha_{\rm lobes} = 0.25$) at low frequencies and very steep ($\alpha_{\rm lobes} = 1.33$) at higher frequencies (Kellermann 1966).

4 OBSERVED SPECTRAL INDEX

We derive the spectral index, α, from the measured radio emission at frequencies $\nu_{\rm TGSS}$ =150 MHz and $\nu_{\rm NVSS}$ =1.4GHz for objects in the TGSS-NVSS common source catalog. For each source we compute the observed spectral index as,

$$\alpha_{\rm obs} = \frac{\log\left(\rm S_{TGSS}/S_{NVSS}\right)}{\log\left(\nu_{\rm NVSS}/\nu_{\rm TGSS}\right)} \ , \tag{3}$$

where $\rm S_{TGSS}$ and $\rm S_{TGSS}$ are, respectively, the flux densities measured by the TGSS and NVSS. As we have seen in §3.1, thermal emission is negligible and this $\alpha_{\rm obs}$ is mainly fixed by the synchrotron component.

We divide our catalog of common sources in two samples. The first low flux (LF) sample contains sources with TGSS and NVSS fluxes below 100 mJy and 20 mJy, respectively[1]. The second high flux (HF) sample includes sources above and equal $\rm S_{TGSS}$ = 100 mJy and $\rm S_{NVSS}$ = 20 mJy. These flux cuts are imposed such as both samples LF and HF contain roughly 50% of sources from our common source catalog. Furthermore, the LF sample is expected to consists of mostly Fanaroff–Riley type I (FR I) galaxies whereas HF sample suppose to contain almost equal number of FR I and FR II galaxies (Wilman et al. 2008).

The non-thermal radio emission consists mainly of synchrotron emission from jets and lobes. The spectral index

[1] Note that $\rm S_{TGSS}$ = 100 mJy corresponds to $\rm S_{NVSS} \approx$ 20 mJy.

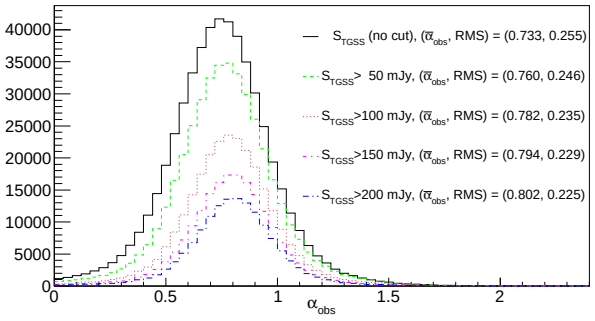
S_TGSS (no cut), (ᾱ_obs, RMS) = (0.733, 0.255)
S_TGSS> 50 mJy, (ᾱ_obs, RMS) = (0.760, 0.246)
S_TGSS>100 mJy, (ᾱ_obs, RMS) = (0.782, 0.235)
S_TGSS>150 mJy, (ᾱ_obs, RMS) = (0.794, 0.229)
S_TGSS>200 mJy, (ᾱ_obs, RMS) = (0.802, 0.225)
α_obs

Figure 2. The NVSS-TGSS extracted radio spectral index with various TGSS flux density cuts. The RMS is the root mean square from $\alpha_{\rm obs}$ distribution.

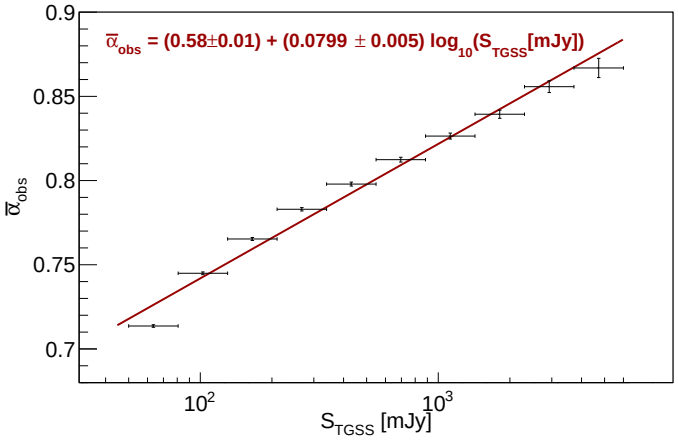

Figure 3. The mean radio spectral index, $\bar{\alpha}_{\rm obs}$, as a function of the source TGSS flux density. The vertical error-bars are the 1σ error in $\bar{\alpha}_{\rm obs}$ in each flux bin. The horizontal error-bars represent the width of each bin.

from systems is not accurately known. For jets the spectral index $\alpha_{\rm jet}$ ranges from 0.5 to 0.9 (Bridle & Perley 1984) and for lobes it may be anywhere between 0.25 to 1.33 (Kellermann 1966). In general we can not isolate the radio emission from jets and lobes, however, the relative contribution from lobes dominates in large sources. For ultra large sources and for continuous energy injection into the lobes, $\alpha_{\rm lobes}$ saturates to the value $\gamma/2$, where γ refers to the electrons in the lobes.

5 RESULTS

5.1 Radio spectral index dependence on flux density

Fig. 2 shows the distribution of $\alpha_{\rm obs}$ for sources with different cuts on $\rm S_{TGSS}$. The "no cut " case includes all 541,195 sources. The number of sources for $S_{\rm TGSS} > 50$, 100, 150, 200 mJy is 424,639; 266,885; 190,830; 147,171 respectively. Although the RMS spread is large, we see a clear trend of steepening of the spectral index with increasing flux. The large RMS spread is expected since individual sources have very different radio emission properties. To explore this further, we sort the sources in logarithmic bins of $\rm S_{TGSS}$ and plot the mean spectral index $\bar{\alpha}_{\rm obs}$ in each bin as a function of the flux density in Fig.3. The observed dependence is fitted by linear parametric form as indicated in the figure. This confirms the earlier hints of spectral index dependence on flux density (Gopal-Krishna & Steppe 1982; Steppe & Gopal-Krishna 1984; Windhorst et al. 1993; Prandoni et al. 2006; Ibar et al. 2009; Ishwara-Chandra et al. 2010; Randall et al. 2012).

5.2 Radio spectral index dependence on size

The size is defined as $\sqrt{ab}$ (in arcsec) where a and b are, respectively, the major and minor axis of the Gaussian fit to the source as given in TGSS. As mentioned in section 4, the observed spectral index consists of radio emission from jets and lobes. Fig. 4 shows $\alpha_{\rm obs}$ as a function of size for LF sample. The mean $\alpha_{\rm obs}$ is computed for sources lying in logarithmic bins of $\sqrt{ab}$. The spectral index increases rapidly with size until $\leqslant 26''$but flattens at larger sizes, becomes

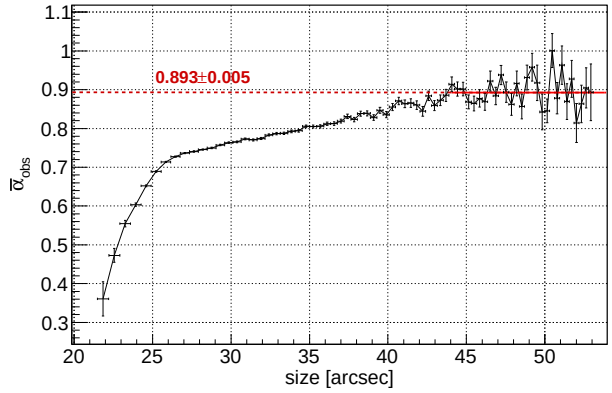

Figure 4. The mean radio spectral index, $\bar{\alpha}_{\rm obs}$, dependence on size ($\sqrt{ab}$) for sources in the LF sample. The vertical and horizontal error-bars represent the uncertainty in $\bar{\alpha}_{\rm obs}$ and the width of the bin. The $\bar{\alpha}_{\rm obs}$ dependence on size saturates very clearly for the sources above 44 arcsec (roughly 350 kpc for $z \approx 1$).

nearly independent of size beyond $\sim 44''$and saturates to the value $\bar{\alpha}_{\rm obs} = 0.890 \pm 0.001$.

Fig. 5 shows $\alpha_{\rm obs}$ versus $\sqrt{ab}$ for the HF sample. The spectral index increases very rapidly with source size and saturates to the limiting value $\bar{\alpha}_{\rm obs} = 0.763 \pm 0.002$ at large sizes ($\gtrsim 35''$). For ultra large sources, the emission is lobe dominated and therefore $\bar{\alpha}_{\rm obs}$ represents the mean spectral index from lobes. If the energy injection in lobes is continuous and the energy losses are only via synchrotron, then, as discussed in §3.2.2, this limiting value yields $\gamma = 2\bar{\alpha}_{\rm obs} = 1.526 \pm 0.004$.

6 SUMMARY AND DISCUSSION

We have computed the radio spectral index from a catalog of about half a million common sources in NVSS and TGSS. We divide the catalog in two flux limited samples LF and HF. The large number of sources enable us to study the spectral index in differential size bins. The spatially integrated

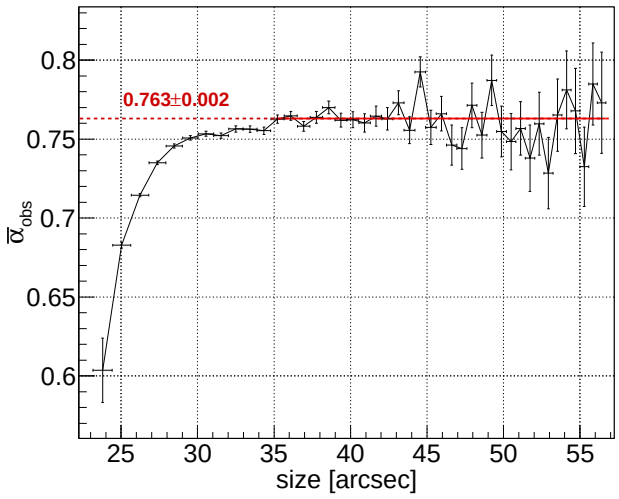

Figure 5. The same as the previous figure but for the HF sources.

radio spectral index, relevant to this work, consists of radio emission from lobes and jets. We explore the source size dependence of observed spectral index and draw the following conclusions:

- We confirm the steepening of the radio spectral index with increasing flux density (Gopal-Krishna & Steppe 1982; Steppe & Gopal-Krishna 1984; Windhorst et al. 1993; Prandoni et al. 2006; Ibar et al. 2009; Ishwara-Chandra et al. 2010; Randall et al. 2012). High flux sources are in general large in size and so the observed flux is mainly from AGN lobes. Emission from lobes is steeper compared with radio emission from jets.
- The spectral index becomes nearly independent of source size above $\sim$ 44 arcsec for LF sample and above $\sim$ 35 arcsec for HF sample. Both samples are hosts of AGNs, the LF sample is presumably dominated by FR I galaxies (Wilman et al. 2008). Assuming that the sources lie at redshifts $z \approx 1$, 44 arcsec size corresponds to $\sim$350 kpc (270 kpc, if at $z = 0.5$). For very compact sources in LF sample, the observed spectral index is flatter ~ 0.4, this hints the significant thermal emission from nucleus in total radio emission for these compact sources.
- HF sample exhibits a very strong dependence of the spectral index on size below $\sim$ 35 arcsec. This is likely due to an increasing fraction of jets and nuclear radio emission in comparison to emission from lobes. The sources with larger sizes reach a saturated spectral index $\bar{\alpha}_{\rm obs} = 0.763 \pm 0.002$. The radio emission from these large sources is lobe dominated and so the observed spectral index can be seen as characteristic of radio emission from lobes.
- The saturated spectral index for LF sample is steeper than HF flux sample. The LF sample is predominantly FR I (Wilman et al. 2008) and the lobes in these galaxies exhibit steepest spectra (Kembhavi & Narlikar 1999), the electrons in lobes are most retarded and aged. Furthermore the slow rise of spectral index with size indicates distorted jet feature of FR I galaxies. Whereas the sharp saturation of spectral index for HF sample, which contains almost equal number of FR I and FR II galaxies (Wilman et al. 2008), indicates very clear domination of radio emission from lobes for these bright galaxies.

ACKNOWLEDGMENTS

We especially thank Adi Nusser and Ari Laor for discussion and their extensive and thoughtful comments on this work. We thank Huib T. Intema (Leiden/NRAO) for help with the TGSS catalog. This work is supported in part at the Technion by a fellowship from the Lady Davis Foundation. We have used CERN ROOT 5.34/21 (Brun et al. 2001) for generating our plots.

References

Biermann P., 1976, A&A, 53, 295
Blandford R. D., Königl A., 1979, ApJ, 232, 34
Bridle A. H., Perley R. A., 1984, ARAA, 22, 319
Brun R., Rademakers F., et al.,, 2001, ROOT web page, `http://root.cern.ch/`
Condon J. J., 1992, ARAA, 30, 575
Condon J. J., Cotton W. D., Greisen E. W., Yin Q. F., Perley R. A., Taylor G. B., Broderick J. J., 1998, AJ, 115, 1693
Condon J. J., Yin Q. F., 1990, ApJ, 357, 97
De Young D. S., 1976, ARAA, 14, 447
Gopal-Krishna Steppe H., 1982, A&A, 113, 150
Ibar E., Ivison R. J., Biggs A. D., Lal D. V., Best P. N., Green D. A., 2009, MNRAS, 397, 281
Intema H. T., Jagannathan P., Mooley K. P., Frail D. A., 2016, Accepted for publication in A&A
Ishwara-Chandra C. H., Sirothia S. K., Wadadekar Y., Pal S., Windhorst R., 2010, MNRAS, 405, 436
Kellermann K. I., 1966, ApJ, 146, 621
Kembhavi A. K., Narlikar J. V., 1999, Quasars and Active Galactic Nuclei An Introduction. Cambridge University Press
Nusser A., Tiwari P., 2015, ApJ, 812, 85
Prandoni I., Parma P., Wieringa M. H., de Ruiter H. R., Gregorini L., Mignano A., Vettolani G., Ekers R. D., 2006, A&A, 457, 517
Randall K. E., Hopkins A. M., Norris R. P., Zinn P.-C., Middelberg E., Mao M. Y., Sharp R. G., 2012, MNRAS, 421, 1644
Steppe H., Gopal-Krishna 1984, A&A, 135, 39
Swarup G., 1991, in Cornwell T. J., Perley R. A., eds, IAU Colloq. 131: Radio Interferometry. Theory, Techniques, and Applications Vol. 19 of Astronomical Society of the Pacific Conference Series, Giant metrewave radio telescope (GMRT). pp 376–380
Tiwari P., Nusser A., 2016, Journal of Cosmology and Astroparticle Physics, 2016, 062
Wilman R. J., Miller L., Jarvis M. J., Mauch T., Levrier F., Abdalla F. B., Rawlings S., Klöckner H.-R., Obreschkow D., Olteanu D., Young S., 2008, MNRAS, 388, 1335
Windhorst R. A., Fomalont E. B., Partridge R. B., Lowenthal J. D., 1993, ApJ, 405, 498